

Assessing the size of spatial extreme events using local coefficients based on excursion sets

Ryan Cotsakis^{1,a,*} Elena Di Bernardino^{2,b} Thomas Opitz^{3,c}

¹ Expertise Center for Climate Extremes (ECCE), Faculty of Business and Economics (HEC) - Faculty of Geosciences and Environment, University of Lausanne, CH-1015 Lausanne, Switzerland,

^a ryan.cotsakis@unil.ch

² Université Côte d'Azur, Laboratoire J.A. Dieudonné, UMR CNRS 7351, Nice,

^b Elena.Di_Bernardino@univ-cotedazur.fr

³ Biostatistics and Spatial Processes, INRAE, Avignon, France; ^c Thomas.Opitz@inrae.fr

January 15, 2025

Abstract

Extreme events arising in georeferenced processes can take various forms, such as occurring in isolated patches or stretching contiguously over large areas, and can further vary with the spatial location and the extremeness of the events. We use excursion sets above threshold exceedances in data observed over a two-dimensional grid of rectangular pixels to propose a general family of coefficients that assess spatial-extent properties relevant for risk assessment, and study five candidate coefficients from this family. These coefficients are defined locally and interpreted as a spatial distance from a reference site where the threshold is exceeded. We develop statistical inference and discuss robustness to boundary effects and resolution of the pixel grid. To statistically extrapolate coefficients towards very high threshold levels, we formulate a semiparametric model and estimate a parameter characterizing how coefficients scale with the quantile level of the threshold. The utility of the new coefficients is illustrated through simulated data, as well as in an application to gridded daily temperature in continental France. We find notable differences in estimated coefficient maps between climate model simulations and observation-based reanalysis.

Keywords: asymptotic independence; climate modeling; extreme value theory; spatial statistics; tail inference.

*The authors gratefully acknowledge that this work has been supported by the French government, through the 3IA Côte d'Azur Investments in the Future project managed by the National Research Agency (ANR) with the reference number ANR-19-P3IA-0002. French weather data based on the SAFRAN reanalysis model were made available by Météo France within its cooperation framework with INRAE.

1 Introduction

Assessing the spatial structure of extreme events is essential for understanding and mitigating complex environmental risks, such as widespread heatwaves, severe droughts, or heavy rainfall episodes. In modern environmental-data settings, data are often available on fine spatial grids with several observations over time, *e.g.*, from climate model output or remote sensing imagery. This increasingly common data format enables the extraction of global shape information of the regions exhibiting threshold exceedances—so-called excursion sets—and provides an opportunity to complement traditional pair-based extremal dependence measures typically applied to relatively small numbers of irregularly-spaced observation locations. The excursion-set-based approach offers several practical advantages. Threshold exceedances are binary indicators, making computations memory-efficient and robust to outliers or censoring of data above extreme levels.

Classical multivariate and spatial Extreme-Value Theory (EVT) focuses extensively on pairwise tail dependence measures and their asymptotic behaviors, *e.g.*, the bivariate extremal coefficient (Schlather & Tawn 2003) or the extremogram (Coles et al. 1999, Davis & Mikosch 2009, Strokorb et al. 2015). These classical measures quantify dependence strength between pairs of locations but cannot fully capture how entire regions may simultaneously exceed critical levels. Moreover, traditional parametric spatial models, often relying on strong assumptions or complex latent-variable structures (*e.g.*, Huser et al. 2024), can be computationally demanding and lack flexibility in capturing intricate spatial patterns. Recent literature suggests that environmental data frequently exhibit decreasing extremal dependence at higher marginal quantiles, so that exceedances become more localized as the threshold grows (Tawn et al. 2018, Huser & Wadsworth 2022, Wadsworth & Tawn 2022). This behavior is typical for asymptotic independence. Formally, for a spatial stochastic process

$X(\mathbf{s})$ with marginal distributions $F_{\mathbf{s}}$, asymptotic independence between two locations $\mathbf{s}_1, \mathbf{s}_2$ means that the conditional exceedance probability $\mathbb{P}(F_{\mathbf{s}_1}(X(\mathbf{s}_1)) > p \mid F_{\mathbf{s}_2}(X(\mathbf{s}_2)) > p)$ tends to zero as the probability threshold p tends to one. Quantifying and inferring such localization patterns from finite data remains challenging.

In the setting where data are numerical and indexed by a two-dimensional rectangular pixel grid, we introduce a novel class of scalar coefficients that directly summarize the geometric properties of excursion set regions exceeding a high, possibly location-dependent threshold (typically, a marginal quantile for a high probability level), conditioned on an exceedance at a given reference site. Each coefficient is constructed to have a natural interpretation as a spatial measure with units of distance. These coefficients distill complex spatial dependence structures into interpretable, local summaries of the spatial “footprint” of extreme events. Unlike methods assessing only pair-based coefficients, these shape-based coefficients intrinsically capture how extremes spread out (or contract) in space, and how this behavior changes as thresholds become more extreme.

The proposed *local excursion-set coefficients* are designed to: (i) adapt naturally to non-stationarity and complex domain boundaries; (ii) remain relatively simple to estimate and interpret from finite samples of the discrete random excursion set; and (iii) reflect the asymptotic behavior of the underlying random field. By assessing how these coefficients change as the threshold increases, we can infer whether the spatial extent of extremes shrinks, remains stable, or even grows in size.

In the present work, rather than advocating for a single summary statistic, we study a family of coefficients, each capturing different aspects of the geometry of exceedance regions. For instance, some coefficients measure how quickly one encounters a non-exceedance point as we move away from the conditioning location, while others gauge the size of the con-

nected exceedance cluster or capture the shape complexity of excursion boundaries. We present five examples of such coefficients in detail, discuss their properties, and provide guidance on their interpretation. Through theoretical considerations and simulation studies, we show that these coefficients can be consistently estimated and can be used to test for asymptotic independence. Indeed, while these five coefficients differ in their practical behavior—some are more conservative in their risk assessment (*i.e.*, leading to relatively larger coefficient values), others are more robust to boundary effects or discretization—they share a fundamental property: under broad conditions, they all evolve at the same rate as thresholds grow large. In other words, at extremely high levels, all five coefficients essentially convey equivalent information regarding the underlying tail dependence structure of the random field. This theoretical equivalence suggests that there is no unique, universally optimal coefficient; each can serve as a diagnostic tool, chosen to best fit the goals of the analysis and the nature of the considered data.

Compared to well-known existing measures of spatial tail dependence, our approach provides a different and complementary perspective. Focusing on global shapes can improve inference in cases where pairwise extremes are rare (*e.g.*, due to a short observation period, low observation frequency, or a very high threshold) or where one aims to characterize how an entire region transitions from relatively large-scale to more localized extremes as thresholds increase. The resulting coefficients can be mapped across space to highlight local differences in the spatial organization of extremes. This could be particularly relevant for climate risk assessments and environmental applications, where understanding the spatial footprint of hazards under future, more severe scenarios is increasingly critical.

The remainder of the paper is organized as follows. Section 2 introduces the local excursion-set coefficients and their theoretical foundations. Section 3 evaluates these coefficients

through simulation studies. Section 4 discusses inference methods for their asymptotic behavior as thresholds increase. Section 5 applies the proposed methodology to French temperature data. Finally, Section 6 provides a discussion of the results and outlines future research directions. Supplementary materials (provided separately) include an additional figure and table.

2 Local excursion sets-based coefficients

2.1 Beyond pair-based dependence measures for extremes

In this section, we introduce a class of geometric coefficients that describe the spatial extent of excursion sets, conditioned on a reference location exceeding a threshold. These coefficients quantify different distance- and area-based aspects of extremal behavior. Their design is guided by the following criteria:

- *Interpretability in terms of spatial distance.* Coefficients should relate directly to distances to capture the notion of *extent*.
- *Computability on large spatial grids.* Modern data sets often include thousands or even millions of grid points, which requires efficient and low-cost algorithms.
- *Local definition in space.* Coefficients should be defined locally, allowing spatial heterogeneity (non-stationarity) in dependence structures to be captured and mapped.
- *Conservatism in risk assessment.* Underestimating the spatial extent of extremes can lead to poor risk management; coefficients should provide conservative summaries.
- *Robustness to boundary effects.* The presence of domain edges should not strongly bias estimates.
- *Robustness to discretization effects.* Coefficients should remain stable when the grid

resolution changes, avoiding artifacts or bias introduced by discretization that is coarse relative to the scale of spatial dependence.

- *Ability to capture asymptotic dependence or independence.* The spatial extent of co-occurring extremes may shrink (asymptotic independence) or remain extensive (asymptotic dependence) as thresholds grow.

Following these considerations, we next introduce in the next section a class of coefficients (see Section 2.2) and highlight their theoretical and practical properties (see Section 2.3).

2.2 Notation and definitions

Let $(\Omega, \mathfrak{F}, \mathbb{P})$ be a probability space, and let $X : \Omega \times \mathbb{R}^2 \rightarrow \mathbb{R}$ be a random field, indexed on a discrete grid. If data are missing at certain locations, the corresponding points are excluded from the grid.

Definition 1 (Discrete domain). *Let $\mathcal{S} \subset \mathbb{Z}^2$ be a finite subset containing the origin $\mathbf{0}$. Define $\mathcal{G} = \{M\mathbf{s} : \mathbf{s} \in \mathcal{S}\}$, where*

$$M = \begin{pmatrix} \Delta_x & 0 \\ 0 & \Delta_y \end{pmatrix}, \quad \Delta_x, \Delta_y > 0.$$

The grid \mathcal{G} represents regularly spaced observation points.

In practice, \mathcal{G} represents raster cells (or image pixels) where $\Delta_x\Delta_y$ is the area of a cell.

Let $\|\cdot\|$ be a norm on \mathbb{R}^2 , inducing a metric on \mathcal{G} . For a threshold function $u : \mathbb{R}^2 \rightarrow \mathbb{R}$, the binary indicator $X(\mathbf{s}) > u(\mathbf{s})$ defines the excursion set as follows.

Definition 2 (Excursion set). *The excursion set of X above the threshold u is*

$$\mathcal{E}_u^{\mathcal{G}, X} = \{\mathbf{s} \in \mathcal{G} : X(\mathbf{s}) > u(\mathbf{s})\}.$$

To summarize the size and shape of $\mathcal{E}_u^{\mathcal{G},X}$, we define functions that map its conditional distribution—given $\mathbf{s} \in \mathcal{E}_u^{\mathcal{G},X}$ for some $\mathbf{s} \in \mathcal{G}$ —to a nonnegative real value. Each of the functions satisfies the following distance-homogeneity property (*i.e.*, rescaling the spatial domain by a positive factor will rescale the function value accordingly), so that their image may be interpreted as a distance, and thus prescribed any unit of distance.

Definition 3 (Distance-homogeneity). *Let $\mathcal{H} \subset \mathbb{R}^2$ be a finite set, $\mathbf{s} \in \mathcal{H}$, and let $\mu_{\mathcal{H}}$ be a probability measure on $\wp(\mathcal{H})$, where \wp denotes the power set. A function $\theta : (\mathcal{H}, \mathbf{s}, \mu_{\mathcal{H}}) \mapsto x \in [0, \infty)$ satisfies distance-homogeneity if, for any $\lambda > 0$,*

$$\theta(\lambda\mathcal{H}, \lambda\mathbf{s}, \mu_{\lambda\mathcal{H}}) = \lambda\theta(\mathcal{H}, \mathbf{s}, \mu_{\mathcal{H}}), \quad (1)$$

where $\lambda\mathcal{H} = \{\lambda\mathbf{h} : \mathbf{h} \in \mathcal{H}\}$ and $\mu_{\lambda\mathcal{H}}(\{\mathcal{A}\}) = \mu_{\mathcal{H}}(\{\lambda^{-1}\mathcal{A}\})$, $\forall \mathcal{A} \in \wp(\lambda\mathcal{H})$.

Definition 4 (Local excursion-set coefficient). *For $\mathbf{s} \in \mathcal{G}$ with $\mathbb{P}(\mathbf{s} \in \mathcal{E}_u^{\mathcal{G},X}) > 0$, a local excursion-set coefficient at \mathbf{s} is defined by $\theta(\mathcal{G}, \mathbf{s}, \mu)$, where θ is any function that satisfies Definition 3, and μ is the law of the conditional excursion set $\mathcal{E}_u^{\mathcal{G},X} \mid \mathbf{s} \in \mathcal{E}_u^{\mathcal{G},X}$. To make the dependence on the threshold function u and the law of the excursion set explicit in the notation, we will write $\theta(\mathbf{s}; \mathcal{E}_u^{\mathcal{G},X}) = \theta(\mathcal{G}, \mathbf{s}, \mu)$.*

The functions θ that satisfy Definition 4 quantify the spatial extent of $\mathcal{E}_u^{\mathcal{G},X}$ conditioned on $\mathbf{s} \in \mathcal{E}_u^{\mathcal{G},X}$, as exemplified by the five coefficients θ_k , $k = 1, \dots, 5$, that we introduce in the following subsection.

2.3 Examples and interpretations

Before introducing the exemplary coefficients, connectivity (based on the adjacency of pixels in the *rook* sense, *i.e.*, along horizontal and vertical directions) and basic geometric quantities are introduced below.

Definition 5 (Connectivity). For $\mathcal{H} \subseteq \mathcal{G}$, points $\mathbf{a}, \mathbf{b} \in \mathcal{H}$ are connected in \mathcal{H} , denoted $\mathbf{a} \stackrel{\mathcal{H}}{\sim} \mathbf{b}$, if there exists a sequence $(\mathbf{s}_1, \dots, \mathbf{s}_n) \subset \mathcal{H}$ such that $\mathbf{s}_1 = \mathbf{a}$, $\mathbf{s}_n = \mathbf{b}$, and $\mathbf{s}_{j+1} - \mathbf{s}_j \in \{(\pm\Delta_x, 0)', (0, \pm\Delta_y)'\}$ for $j = 1, \dots, n-1$.

Definition 6 (Area and perimeter). What we call the area of $\mathcal{H} \subseteq \mathcal{G}$ is given by $A(\mathcal{H}) = |\mathcal{H}| \Delta_x \Delta_y$. The perimeter $P(\mathcal{H})$ is

$$P(\mathcal{H}) = \sum_{\mathbf{s} \in \mathcal{H}} \left(\mathbb{1}_{\{\mathbf{s} + (0, \Delta_y)' \in \mathcal{G} \setminus \mathcal{H}\}} + \mathbb{1}_{\{\mathbf{s} - (0, \Delta_y)' \in \mathcal{G} \setminus \mathcal{H}\}} \right) \Delta_x + \left(\mathbb{1}_{\{\mathbf{s} + (\Delta_x, 0)' \in \mathcal{G} \setminus \mathcal{H}\}} + \mathbb{1}_{\{\mathbf{s} - (\Delta_x, 0)' \in \mathcal{G} \setminus \mathcal{H}\}} \right) \Delta_y.$$

For $\mathbf{s} \in \mathcal{G}$ and $r > 0$, let $\mathcal{B}(\mathbf{s}, r) = \{\tilde{\mathbf{s}} \in \mathcal{G} : \|\tilde{\mathbf{s}} - \mathbf{s}\| \leq r\}$ denote the discrete ball of radius r centered at \mathbf{s} and truncated to \mathcal{G} .

The five coefficients (with possible values in $[0, \infty]$) are as follows (where any quantile function F^{-1} is understood as the generalized inverse of F in the usual way):

1. *Lower extremal range quantiles.* Define $R_*(\mathbf{s}) = \inf\{\|\tilde{\mathbf{s}} - \mathbf{s}\| : \tilde{\mathbf{s}} \in \mathcal{G} \setminus \mathcal{E}_u^{\mathcal{G}, X}\}$. Let $F_1(r; \mathbf{s}) = \mathbb{P}(R_*(\mathbf{s}) \leq r \mid \mathbf{s} \in \mathcal{E}_u^{\mathcal{G}, X})$ be the cumulative distribution function (CDF) of $R_*(\mathbf{s})$, conditional on $\mathbf{s} \in \mathcal{E}_u^{\mathcal{G}, X}$. Then,

$$\theta_1(\mathbf{s}; \mathcal{E}_u^{\mathcal{G}, X}, \alpha) = F_1^{-1}(\alpha; \mathbf{s}), \quad \alpha \in (0, 1).$$

2. *Upper extremal range quantiles.* Define $R^*(\mathbf{s}) = \sup\{\|\tilde{\mathbf{s}} - \mathbf{s}\| : \tilde{\mathbf{s}} \stackrel{\mathcal{E}_u^{\mathcal{G}, X}}{\sim} \mathbf{s}\}$. Let $F_2(r; \mathbf{s}) = \mathbb{P}(R^*(\mathbf{s}) \leq r \mid \mathbf{s} \in \mathcal{E}_u^{\mathcal{G}, X})$. Then,

$$\theta_2(\mathbf{s}; \mathcal{E}_u^{\mathcal{G}, X}, \alpha) = F_2^{-1}(\alpha; \mathbf{s}), \quad \alpha \in (0, 1).$$

3. *Extremal confidence range.* For $r > 0$, let $F_3(r; \mathbf{s}) = \mathbb{E}[A(\mathcal{E}_u^{\mathcal{G}, X} \cap \mathcal{B}(\mathbf{s}, r)) \mid \mathbf{s} \in \mathcal{E}_u^{\mathcal{G}, X}] / A(\mathcal{B}(\mathbf{s}, r))$. Then,

$$\theta_3(\mathbf{s}; \mathcal{E}_u^{\mathcal{G}, X}, \alpha) = \inf\{r > 0 : F_3(r; \mathbf{s}) < \alpha\}, \quad \alpha \in (0, 1).$$

4. *Confidence region range.* For $\alpha \in (0, 1)$, define

$$\theta_4(\mathbf{s}; \mathcal{E}_u^{\mathcal{G}, X}, \alpha) = \sup_{\mathcal{D} \subseteq \mathcal{G}} \{ \sqrt{A(\mathcal{D})/\pi} : \mathbb{P}(\mathcal{D} \subseteq \mathcal{E}_u^{\mathcal{G}, X} \mid \mathbf{s} \in \mathcal{E}_u^{\mathcal{G}, X}) \geq 1 - \alpha \}.$$

5. *Area-perimeter ratio.* If $\mathbb{P}(P(\mathcal{E}_u^{\mathcal{G}, X}) > 0 \mid \mathbf{s} \in \mathcal{E}_u^{\mathcal{G}, X}) > 0$, define

$$\theta_5(\mathbf{s}; \mathcal{E}_u^{\mathcal{G}, X}) = \frac{8\mathbb{E}[A(\mathcal{E}_u^{\mathcal{G}, X}) \mid \mathbf{s} \in \mathcal{E}_u^{\mathcal{G}, X}]}{\pi\mathbb{E}[P(\mathcal{E}_u^{\mathcal{G}, X}) \mid \mathbf{s} \in \mathcal{E}_u^{\mathcal{G}, X}]}.$$

Remark 1. The distribution function $F_1(r; \mathbf{s})$, which underpins θ_1 , is studied in [Cotsakis, Di Bernardino & Opitz \(2024\)](#) and shown to be closely related to the intrinsic volumes of excursion sets. The subset \mathcal{D} used in the construction of θ_4 is analyzed in [Bolin & Lindgren \(2015, 2018\)](#). The coefficient θ_5 involves normalization by the factor $\frac{8}{\pi} = \frac{4}{\pi} \times 2$, which serves two purposes: correcting for the discretization bias inherent in the perimeter length P (see, e.g., [Cotsakis, Di Bernardino & Duval 2024](#)), and aligning the area-perimeter ratio with the radius of an equivalent circular excursion set, specifically $2 \times \frac{\pi r^2}{2\pi r} = r$.

3 Evaluation of the considered coefficients

We now discuss how the coefficients $\theta_1, \dots, \theta_5$ provide complementary summaries of the spatial extent of extremes, balancing conservatism, computational efficiency, and interpretability.

Interpretability. Following from Definition 3, each of the local excursion set coefficients is measured in units of distance. This means that each coefficient scales linearly (up to discretization error) with the amount of spatial rescaling.

The coefficients θ_1 and θ_2 are quantiles of mappings of realizations of $\mathcal{E}_u^{\mathcal{G}, X} \mid \mathbf{s} \in \mathcal{E}_u^{\mathcal{G}, X}$ to real numbers that have clear geometric interpretations. Remark that $R_*(\mathbf{s})$ is the supremum of all $r > 0$ that satisfy $\mathcal{B}(\mathbf{s}, r) \subseteq \mathcal{E}_u^{\mathcal{G}, X}$, and $R^*(\mathbf{s})$ is the infimum of all $r > 0$ that satisfy

$B(\mathbf{s}, r) \supseteq \{\tilde{\mathbf{s}} \in \mathcal{G} : \tilde{\mathbf{s}} \stackrel{\mathcal{E}_u^{\mathcal{G}, X}}{\sim} \mathbf{s}\}$ (see Figure S10 in the Supplementary materials for a graphical illustration).

The extremal confidence range θ_3 is the smallest radius r around \mathbf{s} such that one expects a proportion α of $\mathcal{B}(\mathbf{s}, r)$ to be contained in $\mathcal{E}_u^{\mathcal{G}, X}$. We direct the reader to Bolin & Lindgren (2015) for an interpretation of the confidence region range θ_4 , which is the square root of the area of what they refer to as the *excursion set*—taking on a different meaning from Definition 2—corresponding to the conditional random field $X \mid X(\mathbf{s}) > u(\mathbf{s})$. Finally, the area-perimeter ratio θ_5 provides the radius of circular excursion regions when the grid spacings Δ_x and Δ_y are small in comparison to this radius, correcting for the overestimate of the perimeter of the circle as mentioned in Remark 1.

Locality. Each of the coefficients should be interpreted as a summary of the spatial extent of extremes *conditioned on a threshold exceedance at a site \mathbf{s}* , owing to Definition 4.

Computability. Each θ_k can be estimated via straightforward “plug-in” methods using observations, or Monte Carlo samples from a fitted or hypothesized random field model. Conditional expectations are estimated by sample means that include only realizations of X satisfying the conditioning event. The quantities $R_*(\mathbf{s})$ and $R^*(\mathbf{s})$ can be identified by a breadth-first or depth-first search, starting from \mathbf{s} in $\mathcal{O}(|\mathcal{G}|)$ compute time. The computation of $R^*(\mathbf{s})$ for several \mathbf{s} can be sped up by pre-computing the connected components of each realization of $\mathcal{E}_u^{\mathcal{G}, X}$ and the vertices of the convex hulls of each connected component. Similarly, $R_*(\mathbf{s})$ may be computed for several \mathbf{s} by implementing the Fast Marching Method (Sethian 1996) with the non-exceedances as seeds.

3.1 Numerical study

3.1.1 Setup

We now illustrate the behavior of the five coefficients of Section 2 using simulated data from Gaussian random fields. Let \mathcal{G} be the square lattice $\{-60, \dots, 60\}^2$ with grid spacing $\Delta_x = \Delta_y = 1$.

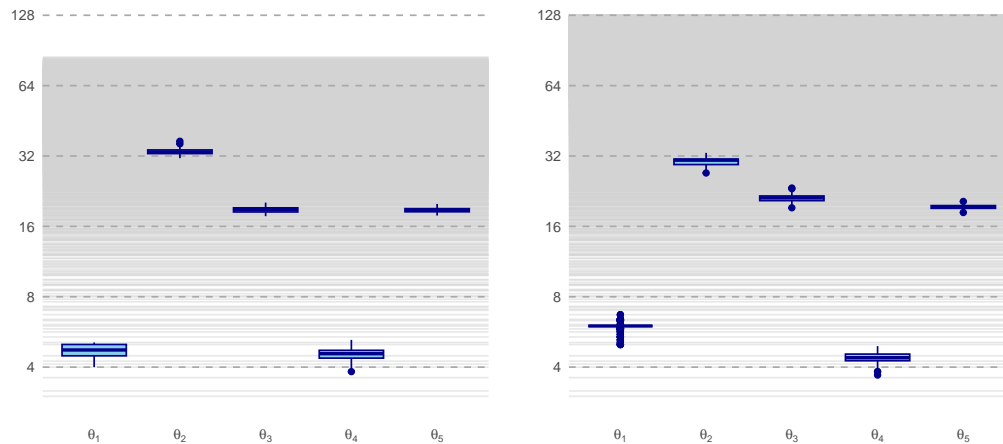


Figure 1: Boxplots of $\theta_k(\mathbf{s}; \mathcal{E}_u^{\mathcal{G}, X}, 0.5)$, for $k = 1, \dots, 4$ and $\theta_5(\mathbf{s}; \mathcal{E}_u^{\mathcal{G}, X})$ for $\mathbf{s} = \mathbf{0}$ (left) and $\mathbf{s} = (60, 0)'$ (right). A gray horizontal line is drawn for each distance from \mathbf{s} where there is a point in \mathcal{G} .

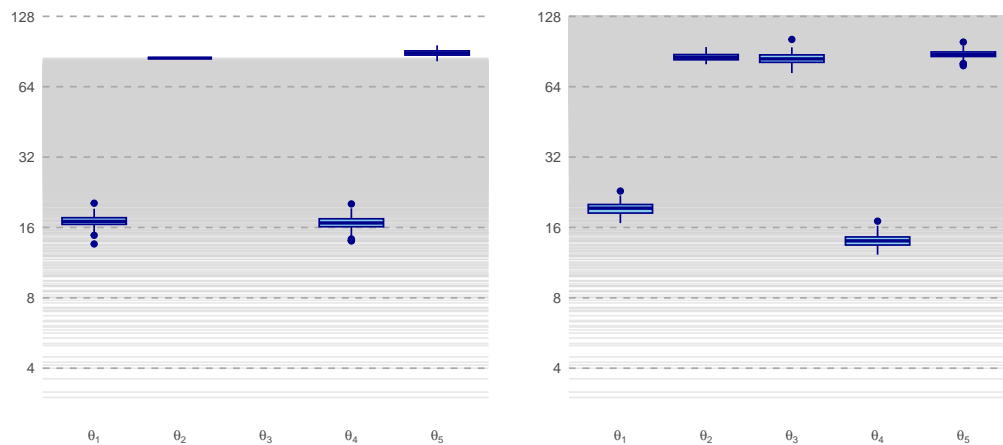


Figure 2: Same as Figure 1 but for $\mathcal{E}_u^{\mathcal{G}, Y}$ instead of $\mathcal{E}_u^{\mathcal{G}, X}$.

We consider a zero-mean, unit-variance, stationary Gaussian random field X on \mathbb{R}^2 with Matérn covariance: $\rho(\mathbf{h}) = \frac{2^{1-\nu}}{\Gamma(\nu)} \left(\frac{\sqrt{2\nu}\|\mathbf{h}\|}{l} \right)^\nu K_\nu \left(\frac{\sqrt{2\nu}\|\mathbf{h}\|}{l} \right)$, $\mathbf{h} \in \mathbb{R}^2$, with regularity $\nu = 2.5$ and range $l = 30$, where K_ν is the modified Bessel function of the second kind. We also define $Y(\mathbf{s}) = X(\frac{\mathbf{s}}{4})$, which stretches the covariance range by a factor of 4.

We select u to be the 99% marginal Gaussian quantile, *i.e.* $\mathbb{P}[X(\mathbf{s}) > u] = 0.01$. Here, since the considered model is stationary, u is constant on \mathcal{G} . We simulate 500 i.i.d. realizations of X , conditionally on X exceeding u at the origin, $\mathbf{s} = \mathbf{0}$. We obtain estimates of $\theta_k(\mathbf{s}; \mathcal{E}_u^{\mathcal{G},X}, 0.5)$, *i.e.*, considering median levels with $\alpha = 0.5$, for $k = 1, \dots, 4$, and of $\theta_5(\mathbf{s}; \mathcal{E}_u^{\mathcal{G},X})$, by approximating probabilities by sample frequencies and expectations by sample means. We repeat this process for 200 bootstrap samples of the 500 independent realizations of $\mathcal{E}_u^{\mathcal{G},X} \mid \mathbf{0} \in \mathcal{E}_u^{\mathcal{G},X}$, and plot (on a logarithmic scale) the 200 resulting estimates of each θ_k , $k = 1, \dots, 5$; results are reported in Figure 1 and interpreted in the following subsection. The analysis is repeated for the excursion set $\mathcal{E}_u^{\mathcal{G},Y}$ in place of $\mathcal{E}_u^{\mathcal{G},X}$ in Figure 2. We also repeat the analysis for both fields using a boundary point $\mathbf{s} = (60, 0)'$ to test for biases induced by the edge of the domain. Table S1 in the Supplementary materials summarizes the median and standard deviation of the logarithm of the estimates of θ_k across different ranges l in the Matérn covariance and locations \mathbf{s} .

3.1.2 Results and discussion

Several key observations emerge from the analysis of Figures 1–2.

Conservatism. Among the five coefficients, θ_2 is the most conservative, consistently yielding the highest values. This makes it a relevant choice for risk assessment when understating the extent of an extreme event is problematic. However, this conservatism comes with trade-offs, particularly its sensitivity to boundary effects, as evidenced by the left plot of Figure 2, where the median is consistently the maximum allowed value. In

contrast, both θ_1 and θ_4 severely underrate the extent of an extreme event compared to the other coefficients and could lead to erroneous interpretation of the risk exposure.

Robustness to edge effects. The coefficient θ_5 stands out as the most robust to boundary effects, showing only negligible shifts when comparing results at the center of the domain $\mathbf{s} = \mathbf{0}$ and at the boundary $\mathbf{s} = (60, 0)'$. In addition, this coefficient does not suffer from missing data at large distances from the conditioning location. By contrast, in Figure 2, the left plot shows the sensitivity of θ_2 and θ_3 to domain truncation— θ_3 is not even defined, as the estimated $F_3(\cdot; \mathbf{0})$ never drops below 0.5.

Robustness to discretization. As Y has a correlation structure that is four times the extent of X , we expect that the quantities in Figure 2 should be four times those Figure 1. Deviations from this factor of four are the result of spatial discretization error and statistical error—the latter can be accounted for by the width of the boxplots. The area-perimeter ratio θ_5 performs well in this regard. Aside from edge truncation effects, θ_3 also seems to reflect the factor of four in the right-hand side of the two plots. In Figure 1, on the left, we see that θ_1 is comparable in size to Δ_x and Δ_y , and its permissible values are quite limited due to the few number of points in \mathcal{G} with a corresponding magnitude of about 5.

Overall, θ_5 emerges as a well-balanced coefficient, performing reliably across all categories. It is moderately conservative, robust to edge effects, and scales consistently with changes in spatial dependence. While θ_2 has an intuitive interpretation and is the most conservative of the coefficients, its sensitivity to edge effects limits its utility in quantifying asymptotic independence, especially when the domain size is comparable to the size of the extremes. For each of the coefficients, the low variability (on a log-scale) is indicative of the coefficient's ability to capture the extent of spatial extremes, and track the evolution as the threshold changes. We elaborate on this in the following section.

Code to reproduce Figures 1–2 is provided at <https://github.com/pony-helping-treat/Local-Excursion-Set-Coefficients>.

If there is any specific limit or scaling behavior one wishes to highlight in real-world applications (*e.g.*, reliance on large-domain asymptotics), care must be taken to assess possible discretization artifacts when Δ_x and Δ_y are not sufficiently small. This point will be further developed in Section 4 below.

4 Inference for asymptotic behavior at increasingly extreme thresholds

This section examines the asymptotics of the coefficients θ_k as the threshold u grows. For each location $\mathbf{s} \in \mathcal{G}$, let $F_{X(\mathbf{s})}$ denote the CDF of $X(\mathbf{s})$. Then, for each $p \in (0, 1)$, define the quantile threshold function $u_p : \mathbb{R}^2 \rightarrow \mathbb{R}$ by $u_p(\mathbf{s}) = F_{X(\mathbf{s})}^{-1}(p)$.

4.1 Convergence of the considered coefficients

We consider excursion sets where the dependence structure of the underlying random field is appropriately scaled by a function $\sigma(p)$ so that a limit is obtained as $p \rightarrow 1$. In this way, the spatial extent of the extremes of random fields with no scaling must evolve like the reciprocal of σ . In what follows, we show that the coefficients θ_k can be used to uncover the asymptotic behavior of $\sigma(p)$ as $p \rightarrow 1$. Moreover, we propose a model for σ that gives rise to a more accurate inference strategy for the local excursion set coefficients θ_k at very extreme levels where excursions are scarce or yet unobserved in data.

Definition 7. *Let $\sigma : (0, 1) \rightarrow (0, \infty)$ be a scaling function and let $p \in (0, 1)$. Let us define*

$$\mathcal{E}_p^{\mathcal{G}} = \left\{ \mathbf{s} \in \mathcal{G} : X \left(\frac{\mathbf{s}}{\sigma(p)} \right) > u_p \left(\frac{\mathbf{s}}{\sigma(p)} \right) \right\}. \quad (2)$$

The set $\mathcal{E}_p^{\mathcal{G}}$ may be interpreted as the excursion set of the random field $Y : \Omega \times \mathbb{R}^2 \rightarrow \mathbb{R}$, defined by $Y(\mathbf{s}) = X\left(\frac{\mathbf{s}}{\sigma(p)}\right)$, $\mathbf{s} \in \mathbb{R}^2$, at the threshold $u_p^Y : \mathbb{R}^2 \rightarrow \mathbb{R}$ defined by $u_p^Y(\mathbf{s}) = u_p\left(\frac{\mathbf{s}}{\sigma(p)}\right)$. For any fixed $p \in (0, 1)$, the distribution of the conditional random set $\mathcal{E}_p^{\mathcal{G}} \mid \mathbf{0} \in \mathcal{E}_p^{\mathcal{G}}$ on $\wp(\mathcal{G})$ is denoted ν_p .

Note that $\mathbf{0} \in \mathcal{G}$ by construction in Definition 1.

Assumption 1. Suppose that σ , the scaling factor used to define $\mathcal{E}_p^{\mathcal{G}}$ in (2), is chosen such that $\forall \mathfrak{A} \in \wp(\wp(\mathcal{G}))$ the probability measure ν_p on $\wp(\mathcal{G})$ satisfies

$$\nu_p(\mathfrak{A}) = \mathbb{P}\left(\mathcal{E}_p^{\mathcal{G}} \in \mathfrak{A} \mid \mathbf{0} \in \mathcal{E}_p^{\mathcal{G}}\right) \xrightarrow[p \rightarrow 1]{} \nu(\mathfrak{A}),$$

with ν a non-degenerate limiting measure.

Remark 2 (On Assumption 1). One can adapt the proofs of Propositions 2 and 3 in [Cotsakis, Di Bernardino & Opitz \(2024\)](#) in order to show that both Gaussian and regularly varying (RV) random fields satisfy Assumption 1. Indeed, one can select the scaling function as $\sigma(p) = u_p(\mathbf{0})$ (*i.e.*, linear behavior in the threshold) for stationary Gaussian random fields and $\sigma(p) = 1$ (*i.e.*, constant behavior in the threshold) for RV random fields. For details on RV random fields, see [Hult & Lindskog \(2005, 2006\)](#). Coordinate rescalings of Gaussian processes that lead to nondegenerate extreme-value limits have also been studied in the context of max-stable processes (Section 6, [Kablichko et al. 2009](#)).

Each of the coefficients θ_k , $k = 1, \dots, 5$, is defined in terms of a location $\mathbf{s} \in \mathcal{G}$ and the excursion set $\mathcal{E}_u^{\mathcal{G}, X}$. By replacing $\mathcal{E}_u^{\mathcal{G}, X}$ in the definition of our five coefficients with $\mathcal{E}_p^{\mathcal{G}}$ in (2), we obtain (with some abuse of notation) the coefficients $\theta_k(\mathbf{0}; \mathcal{E}_p^{\mathcal{G}}, \alpha)$, for $k = 1, \dots, 4$, and $\theta_5(\mathbf{0}; \mathcal{E}_p^{\mathcal{G}})$. Under Assumption 1, let $\mathcal{E}^{\mathcal{G}}$ be the limiting random element of $\wp(\mathcal{G})$ with distribution ν , and define $\theta_k(\mathbf{0}; \mathcal{E}^{\mathcal{G}}, \alpha)$, for $k = 1, \dots, 4$, and $\theta_5(\mathbf{0}; \mathcal{E}^{\mathcal{G}})$ accordingly.

Finally, the following assumption ensures that each θ_k , $k = 1, \dots, 4$, is stable for small changes in the hyperparameter α .

Assumption 2. Fix $\alpha \in (0, 1)$. Suppose that $\theta_k(\mathbf{0}; \mathcal{E}^{\mathcal{G}}, \tilde{\alpha})$ is continuous in $\tilde{\alpha}$ in a small neighborhood of α , for each $k = 1, \dots, 4$.

In the following, under Assumptions 1–2, each of the five coefficients is studied for $p \rightarrow 1$.

Proposition 1. Fix $\alpha \in (0, 1)$. Let $\mathcal{E}_p^{\mathcal{G}}$ be as in (2). Then,

- under Assumption 1, $\theta_5(\mathbf{0}; \mathcal{E}_p^{\mathcal{G}}) \xrightarrow{p \rightarrow 1} \theta_5(\mathbf{0}; \mathcal{E}^{\mathcal{G}})$;
- under Assumptions 1 and 2, $\theta_k(\mathbf{0}; \mathcal{E}_p^{\mathcal{G}}, \alpha) \xrightarrow{p \rightarrow 1} \theta_k(\mathbf{0}; \mathcal{E}^{\mathcal{G}}, \alpha)$, for $k = 1, \dots, 4$.

Proof. By the finiteness of \mathcal{G} , the convergence of $\mathcal{E}_p^{\mathcal{G}} \mid \mathbf{0} \in \mathcal{E}_p$ to $\mathcal{E}^{\mathcal{G}}$ implies the convergence of the conditional expectation of any real function of $\mathcal{E}_p^{\mathcal{G}}$ to the expectation for $\mathcal{E}^{\mathcal{G}}$. Moreover, the finiteness of \mathcal{G} implies that the set $\{\theta_k(\mathbf{0}; \mathcal{E}_p^{\mathcal{G}}, \alpha) : p \in (0, 1)\}$, namely \mathcal{J} , has finite cardinality for all $k = 1, \dots, 4$. For $p \in (0, 1)$, the coefficients $\theta_k(\mathbf{0}; \mathcal{E}_p^{\mathcal{G}}, \alpha)$ are monotonic in α , and so we may partition $(0, 1)$ into the intervals $(\{\alpha \in (0, 1) : \theta_k(\mathbf{0}; \mathcal{E}_p^{\mathcal{G}}, \alpha) = j\})_{j \in \mathcal{J}}$. Under Assumption 1, these intervals converge to $(\{\alpha \in (0, 1) : \theta_k(\mathbf{0}; \mathcal{E}^{\mathcal{G}}, \alpha) = j\})_{j \in \mathcal{J}}$ as $p \rightarrow 1$, and under Assumption 2, α is an interior point of one of the limiting intervals. \square

In the following, θ denotes any one of the coefficients θ_k for $k = 1, \dots, 5$, and the dependence on the hyperparameter α (in the case $k \neq 5$) is not written explicitly. The following lemma links the scaling behaviors of the coefficient, the excursion set and the grid.

Lemma 1. The following equivalences hold for $p \in (0, 1)$ under Assumption 1:

$$(a) \quad \lambda \theta(\mathbf{0}; \mathcal{E}_p^{\mathcal{G}}) = \theta(\mathbf{0}; \lambda \mathcal{E}_p^{\mathcal{G}}), \quad \forall \lambda > 0.$$

$$(b) \quad \frac{1}{\sigma(p)} \mathcal{E}_p^{\mathcal{G}} = \mathcal{E}_{u_p}^{\mathcal{G}/\sigma(p), X} \text{ almost surely.}$$

$$(c) \quad \theta(\mathbf{0}; \mathcal{E}_p^{\mathcal{G}}) = \sigma(p) \theta(\mathbf{0}; \mathcal{E}_{u_p}^{\mathcal{G}/\sigma(p), X}).$$

Proof. Item (a) is a direct application of Equation (1), where $\theta(\mathbf{0}; \lambda \mathcal{E}_p^{\mathcal{G}})$ should be interpreted as the image of $(\lambda \mathcal{G}, \mathbf{0}, \mu)$ under θ where μ is the law of $\lambda \mathcal{E}_p^{\mathcal{G}} \mid \mathbf{0} \in \mathcal{E}_p^{\mathcal{G}}$ (see Definition 4). Item (b) holds almost surely since $\frac{1}{\sigma(p)} \mathcal{E}_p^{\mathcal{G}} = \left\{ \frac{\mathbf{s}}{\sigma(p)} : \mathbf{s} \in \mathcal{G}, X\left(\frac{\mathbf{s}}{\sigma(p)}\right) > u_p\left(\frac{\mathbf{s}}{\sigma(p)}\right) \right\} = \left\{ \tilde{\mathbf{s}} \in \frac{1}{\sigma(p)} \mathcal{G} : X(\tilde{\mathbf{s}}) > u_p(\tilde{\mathbf{s}}) \right\} = \mathcal{E}_{u_p}^{\mathcal{G}/\sigma(p), X}$. Item (c) follows directly from items (a) and (b) with $\lambda = 1/\sigma(p)$. \square

Results above show how, under Assumptions 1 and 2, one can choose an appropriate scaling function σ such that the limit coefficients can be made non-zero constants. Alternatively, one can choose the grid spacing parameters Δ_x and Δ_y sufficiently small, as we will show in the next section (see Assumption 4 below).

4.2 Inference of the scaling index

Assumption 3 below is motivated by the behavior of Gaussian and regularly varying random fields and can be interpreted as a general model for the behavior of the appropriate scaling factor $\sigma(p)$ as a function of the threshold u_p .

Assumption 3 (Scaling index β). *There exists $\beta \in \mathbb{R}$ such that for all $a > 0$, Assumption 1 holds for \mathcal{E}_p in (2) defined by a function σ that satisfies*

$$\lim_{x \rightarrow \infty} \frac{\sigma(1 - e^{-ax})}{\sigma(1 - e^{-x})} = a^\beta. \quad (3)$$

Remark 3 (On Assumption 3). Equation (3) is equivalent to asking that the function $f : x \mapsto \sigma(1 - e^{-x})$, $x \in (0, \infty)$ is regularly varying with index β . Since this corresponds to a marginal quantile at $p = 1 - e^{-x}$, we can x as the marginal log-return time. The function f is σ composed with the CDF of a standard exponential random variable. Therefore, if $X(\mathbf{0})$ is standard exponential, then $u_p(\mathbf{0})$ corresponding to $p = 1 - e^{-x}$ is equal to x , $\forall x \in (0, \infty)$. Thus, in this case, f maps $u_p(\mathbf{0})$ to $\sigma(p)$, relating the threshold to the appropriate scaling

factor. Analogous to considerations in Remark 2, notice that Assumption 3 is satisfied by Gaussian random fields with $\beta = 1/2$ and RV random fields with $\beta = 0$.

Assumption 4. Let $p \in (0, 1)$. For any $\lambda, \epsilon > 0$, suppose that the grid \mathcal{G} may be chosen such that

$$(a) \quad \left| \theta(\mathbf{0}; \mathcal{E}_{u_p}^{\lambda \mathcal{G}, X}) - \theta(\mathbf{0}; \mathcal{E}_{u_p}^{\mathcal{G}, X}) \right| < \epsilon,$$

and that under Assumption 1, the scaling function σ may be normalized such that

$$(b) \quad \theta(\mathbf{0}; \mathcal{E}^{\mathcal{G}}) > 0.$$

Theorem 1. Suppose that for all $p_1, p_2 \in (0, 1)$ with $p_1 < p_2$, there exists a corresponding \mathcal{G} satisfying Assumptions 1-4. Then, for any $\epsilon > 0$ and $a > 1$, there exists $p_0 \in (0, 1)$ such that for all $p_1, p_2 \in (p_0, 1)$ with $\log(1 - p_2) = a \log(1 - p_1)$, it is possible to choose \mathcal{G} such that

$$\left| -\beta - \frac{\log \theta(\mathbf{0}; \mathcal{E}_{u_{p_2}}^{\mathcal{G}, X}) - \log \theta(\mathbf{0}; \mathcal{E}_{u_{p_1}}^{\mathcal{G}, X})}{\log x_2 - \log x_1} \right| < \epsilon,$$

where $x_i = -\log(1 - p_i)$ for $i = 1, 2$, and β is the scaling index in (3).

Proof of Theorem 1. Assumption 4 (b) together with Item (c) in Lemma 1 and Proposition 1 imply $\log \sigma(p) + \log \theta(\mathbf{0}; \mathcal{E}_{u_p}^{\mathcal{G}/\sigma(p), X}) \xrightarrow{p \rightarrow 1} \log \theta(\mathbf{0}; \mathcal{E}^{\mathcal{G}})$. Therefore,

$$\left| \left(\log \sigma(p_1) + \log \theta(\mathbf{0}; \mathcal{E}_{u_{p_1}}^{\mathcal{G}/\sigma(p_1), X}) \right) - \left(\log \sigma(p_2) + \log \theta(\mathbf{0}; \mathcal{E}_{u_{p_2}}^{\mathcal{G}/\sigma(p_2), X}) \right) \right| \quad (4)$$

can be made arbitrarily close to 0 for sufficiently large p_0 . Then, by adding and subtracting $\log \theta(\mathbf{0}; \mathcal{E}_{u_{p_1}}^{\mathcal{G}/\sigma(p_2), X})$ to (4), we have

$$\begin{aligned} \log \sigma(p_1) - \log \sigma(p_2) &\approx \log \theta(\mathbf{0}; \mathcal{E}_{u_{p_2}}^{\mathcal{G}/\sigma(p_2), X}) - \log \theta(\mathbf{0}; \mathcal{E}_{u_{p_1}}^{\mathcal{G}/\sigma(p_2), X}) \\ &\quad + \left(\log \theta(\mathbf{0}; \mathcal{E}_{u_{p_1}}^{\mathcal{G}/\sigma(p_2), X}) - \log \theta(\mathbf{0}; \mathcal{E}_{u_{p_1}}^{\mathcal{G}/\sigma(p_1), X}) \right), \end{aligned} \quad (5)$$

where \approx means that the two expressions can be made arbitrarily close to the same value by choice of p_0 . Moreover, by Assumption 3, we have

$$\log \sigma(p_1) - \log \sigma(p_2) \approx -\beta \log a = -\beta(\log x_2 - \log x_1).$$

By Assumption 4 (a), \mathcal{G} may be chosen such that $|\log \theta(\mathbf{0}; \mathcal{E}_{u_{p_1}}^{\mathcal{G}/\sigma(p_2), X}) - \log \theta(\mathbf{0}; \mathcal{E}_{u_{p_1}}^{\mathcal{G}/\sigma(p_1), X})|$ is negligible in comparison to $\log x_2 - \log x_1$. Therefore, we may divide the right-hand side of (5) by $\log x_2 - \log x_1$ to obtain

$$\frac{\log \theta(\mathbf{0}; \mathcal{E}_{u_{p_2}}^{\mathcal{G}/\sigma(p_2), X}) - \log \theta(\mathbf{0}; \mathcal{E}_{u_{p_1}}^{\mathcal{G}/\sigma(p_2), X})}{\log x_2 - \log x_1} \approx -\beta.$$

Notice that, without loss of generality, we may assume that $\sigma(p_2) = 1$, since rescaling σ and \mathcal{G} by the same positive constant maintains Assumptions 1–4. \square

Theorem 1 provides a method to infer the scaling index of the appropriate scaling factor σ . Indeed, by studying the evolution of any of the five considered coefficients as a function of the threshold u , we may deduce the scaling index β as the slope of a linear regression on appropriately rescaled axes, which in effect, determines how the spatial extent of extreme events tends to decrease at high thresholds.

Remark 4 (On grid spacing). The result assumes that Δ_x, Δ_y are small enough to approximate continuous scaling behavior. Unsurprisingly, if the grid is coarse, discretization effects may obscure the true asymptotics, leading to incorrect estimates of β .

4.3 Estimation strategy

We present our general procedure to infer the coefficients at a location \mathbf{s} by first empirically evaluating them at several threshold levels u and then fitting a linear regression based on Assumption 3 and Theorem 1. We illustrate the approach by generating 2000 independent realizations of a random field X (with X and \mathcal{G} are as defined in Section 3.1),

each conditioned on the event $\{X(\mathbf{0}) > 1.75\}$. For each realization, we compute the five coefficients

$$\theta_k(\mathbf{0}; \mathcal{E}_u^{\mathcal{G}, X}, 0.5), \quad k = 1, \dots, 4, \quad \text{and} \quad \theta_5(\mathbf{0}; \mathcal{E}_u^{\mathcal{G}, X}),$$

evaluated at several threshold levels u . Below, we detail each step of the procedure.

i) Transforming thresholds and gathering estimates. We select a range of threshold levels u such that $\log(-\log(1 - F_{X(\mathbf{0})}(u)))$ is spaced across a suitable range of values—sufficiently high to capture extreme behavior but not so high that estimates become unduly noisy or unstable. Let us denote u_1, \dots, u_J these thresholds. For each u , we use all 2000 conditional realizations of X to compute $\hat{\theta}_k(\mathbf{0}; \mathcal{E}_u^{\mathcal{G}, X}, 0.5)$, $k = 1, \dots, 4$, and $\hat{\theta}_5(\mathbf{0}; \mathcal{E}_u^{\mathcal{G}, X})$. This yields a point estimate of each coefficient at each threshold u_j , for $j \in \{1, \dots, J\}$.

ii) Bootstrapping for variance. To quantify uncertainty in each $\hat{\theta}_k$, we employ a non-parametric bootstrap:

- a) We draw a bootstrap sample of the 2000 conditional realizations with replacement, and compute all $\hat{\theta}_k$ at each u_j on this bootstrap sample.
- b) We repeat the above step 200 times to obtain a bootstrap distribution for each $\hat{\theta}_k$, for each threshold u_j , for $j \in \{1, \dots, J\}$.

From these bootstrap distributions, we estimate the variance of $\log \hat{\theta}_k$ for each $k = 1, \dots, 5$ and u_1, \dots, u_J . These variances guide the weights in our subsequent linear regression and inform our confidence intervals.

iii) Weighted linear regression in log scale. We examine how $\hat{\theta}_k(\mathbf{0}; \mathcal{E}_u^{\mathcal{G}, X})$ changes with u by fitting a weighted linear regression. Concretely, using covariate-observation pairs

$$\left\{ \left(\log(-\log(1 - F_{X(\mathbf{0})}(u_j))), \log \hat{\theta}_k(\mathbf{0}; \mathcal{E}_{u_j}^{\mathcal{G}, X}) \right) : j = 1, \dots, J \right\},$$

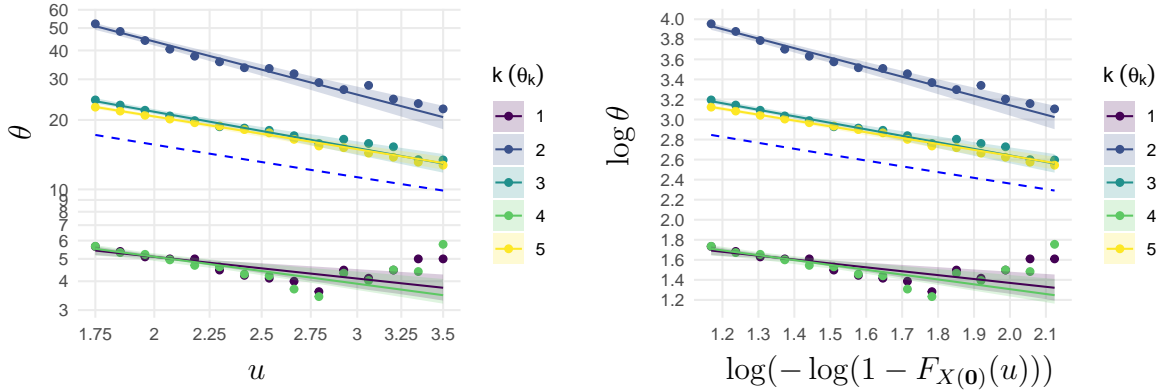


Figure 3: Illustration of the estimation strategy (see Section 4.3) carried out for the five considered local excursion set coefficients. The estimates $\hat{\theta}_k$ are displayed by dots, the fitted weighted linear regressions by lines. Twice the value of the expected area of $\{\mathbf{s} \in [-60, 60]^2 : X(\mathbf{s}) > u\}$ divided by the expected length of $\{\mathbf{s} \in [-60, 60]^2 : X(\mathbf{s}) = u\}$ is shown as a dashed blue curve. Both panels display the same information but with different axes labels, so that the regression coefficients may be read off of the plot on the right.

we perform a weighted least-squares, linear fit, with the j th weight set to the inverse of the bootstrap variance of $\log \hat{\theta}_k(\mathbf{0}; \mathcal{E}_{u_j}^{\mathcal{G}, X})$. This downweights threshold levels whose coefficient estimates exhibit higher uncertainty.

iv) Bootstrapping for confidence intervals. The fitted regression line provides an “improved” estimate of θ_k at *any* threshold u . We then construct 95% confidence intervals around this fitted line by repeating Step 3 for each of the 200 bootstrap samples of $\hat{\theta}_k$ computed in Step 2. In the resulting plots (see Figure 3), we highlight these confidence intervals to give a visual assessment of the precision of our improved estimates.

In Figure 3, we observe that performing a linear regression on appropriately rescaled axes, in accordance with Theorem 1, yields similar slope estimates across all coefficients. This consistency shows how each coefficient captures the same underlying degree of asymptotic independence. The regression lines decrease at a rate similar to the dashed blue curve

that shows the theoretical value of θ_5 —calculated from the Gaussian kinematic formula (Adler & Taylor 2007, Theorem 15.9.5)—as the grid spacing approaches zero. Although the estimates of θ_5 tend to slightly overestimate the theoretical values—attributed to the discrete nature of \mathcal{G} —the estimated slopes remain in close agreement with the theoretical expectations. Specifically, θ_5 exhibits a slope of -0.59 with a 95% confidence interval of $[-0.66, -0.52]$, which is near the theoretical slope that remains approximately -0.58 in the range of the displayed axes (asymptotically, this slope tends to -0.5 as $u \rightarrow \infty$). Larger deviations are primarily observed for the smaller coefficients, where discretization effects play a more important role.

5 Application to French temperature data

Temperature typically varies relatively smoothly in geographic space (Perkins et al. 2012). Extreme events, such as heatwaves, can stretch over large areas. Assessing the spatial extent of such extremes, and how it changes with event frequency, is critical for understanding the compound risks they impose.

In this section, we illustrate and compare the proposed local excursion-set coefficients on two datasets of daily-average summer (June–August) temperatures over mainland France for their overlap period covering years 1970–2005. The majority of temperature extremes manifest in these summer months. Both datasets are defined on the same $8\text{km} \times 8\text{km}$ grid, denoted \mathcal{F} , in the Lambert-II projection. The two datasets under consideration are:

- **Reanalysis:** Derived from the SAFRAN reanalysis model (Vidal et al. 2010), which integrates observational data with numerical weather prediction models to provide a comprehensive historical temperature record.

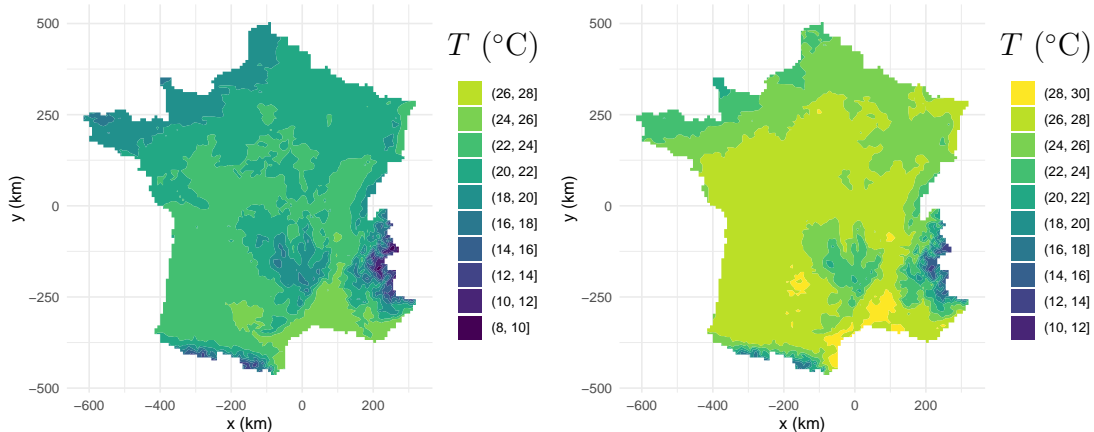


Figure 4: Estimated quantile thresholds $u_p(\mathbf{s})$ for $p = 0.86$ (left) and $p = 0.99$ (right) across mainland France based on the Reanalysis dataset.

- **Simulation:** Generated for the CMIP5 historical experiment using the coupled IPSL-WRF global/regional climate model. This dataset is one of the reference models selected by the French weather service (Météo France) for studying climate change impacts (<http://www.drias-climat.fr/>).

We perform the same analyses for each of the two datasets, ensuring that any differences in the results can be attributed to either statistical uncertainties (which we assess) or more fundamental differences in the distributional properties of the two datasets.

For each location $\mathbf{s} \in \mathcal{F}$, we compute the empirical p -quantiles $u_p(\mathbf{s})$ for several p ranging from 0.86 to 0.99 using the 36 summer seasons (approximately 3300 days) and we perform our analysis on the excursion sets $\mathcal{E}_{u_p}^{\mathcal{F}, X} = \{\mathbf{s} \in \mathcal{F} : X(\mathbf{s}) > u_p(\mathbf{s})\}$, where X denotes either the Reanalysis or Simulation dataset.

Figure 4 illustrates the estimated 0.86 and 0.99 quantiles for the Reanalysis dataset, highlighting the spatial variability driven by topographic and climatic factors.

From the quantile maps for each dataset, we are able to compute the excursion set $\mathcal{E}_{u_p}^{\mathcal{F}, X}$ for each quantile level p on each day. We exhibit the excursion sets, with those for relatively

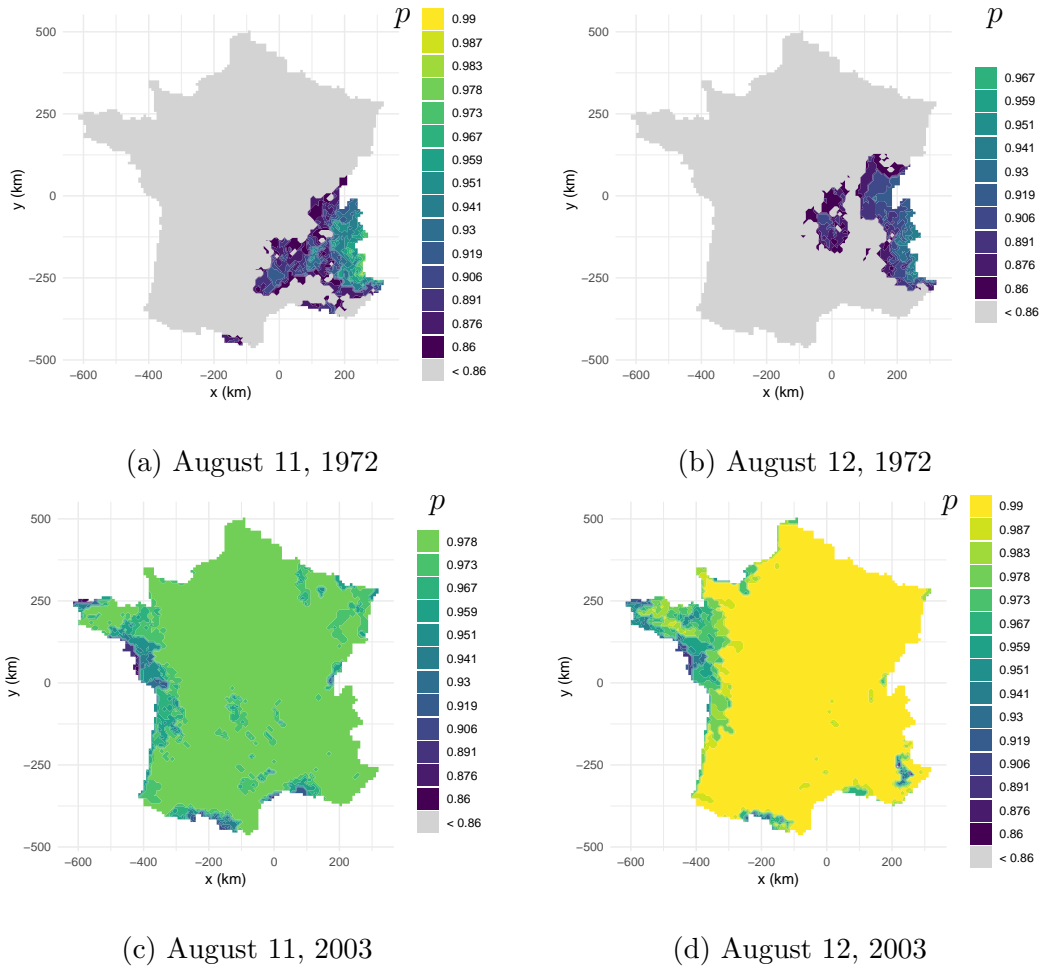


Figure 5: $\mathcal{E}_{u_p}^{\mathcal{F}, X}$, for several p , observed on four different days. This corresponds to displaying the temperature over France on uniform margins, binned using the chosen values of p .

larger p nested within those for relatively smaller p , corresponding to the Reanalysis dataset on four different days in Figure 5, with the two days in 2003 being part of one of the most severe heatwaves of recent decades.

5.1 Comparative analysis of local excursion set coefficients

Following the estimation strategy outlined in Section 4.3, we compute the parameters of the linear models for the median upper extremal range $\theta_2(\mathbf{s}; \mathcal{E}_{u_p}^{\mathcal{F}, X}, 0.5)$ and the Area-Perimeter ratio $\theta_5(\mathbf{s}; \mathcal{E}_{u_p}^{\mathcal{F}, X})$ separately for each $\mathbf{s} \in \mathcal{F}$. Given the temporal dependence inherent in

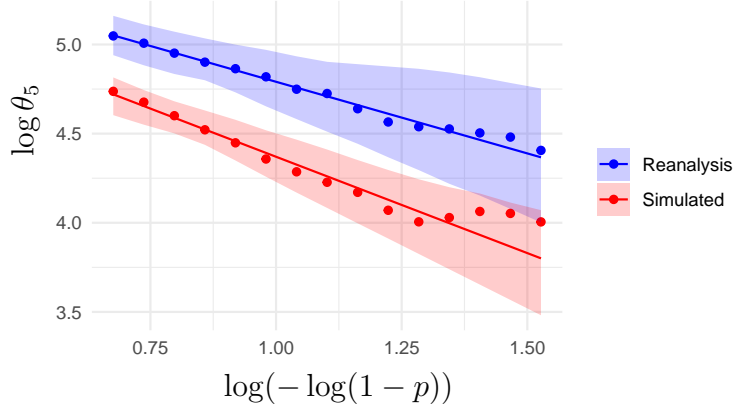


Figure 6: Estimates of $\theta_5(\mathbf{0}; \mathcal{E}_{u_p}^{\mathcal{F}, X})$ for both SAFRAN Reanalysis data (shown in blue) and for CMIP5 Simulation data (shown in red). A linear regression serves as an improved estimate of $\theta_5(\mathbf{0}; \mathcal{E}_{u_p}^{\mathcal{F}, X})$, and the corresponding 95% confidence interval (computed using stationary block bootstrap with mean block size of 10) is highlighted for each dataset.

daily temperature data, a stationary block bootstrap with a mean block size of 10 days is used when computing variances and confidence intervals (Politis & Romano 1994).

The resulting fits of $\theta_5(\mathbf{s}; \mathcal{E}_{u_p}^{\mathcal{F}, X})$ for $\mathbf{s} = \mathbf{0}$ (the origin of the coordinate system of Figure 5) are shown in Figure 6. The difference between the model for the Reanalysis data and the Simulated data is statistically significant, as the confidence intervals (calculated from repeated linear fits using the bootstrap procedure) are non-overlapping for most of the considered region of threshold values. The two regression lines for $\log \theta_5$ are separated by at least 0.25, such that estimated coefficients are at least 25% higher for Reanalysis data. The possible discretization bias at high quantile levels p (especially in Simulation data) is attenuated through the weighting procedure when calculating the linear fits. The discrepancies between the two datasets may stem from inherent differences in how the climate model (Simulation) represents physical processes governing extreme temperature events. Such biases could have profound implications for risk assessments and climate

projections relying on model simulations.

5.1.1 Area-perimeter ratio θ_5

Figure 7 presents a map of the estimated area-perimeter ratio $\theta_5(\mathbf{s}; \mathcal{E}_{u_p}^{\mathcal{F}, X})$ at the 99th percentile threshold ($p = 0.99$) for both the Reanalysis and Simulation datasets. The Reanalysis dataset consistently exhibits larger θ_5 values compared to the Simulation dataset. Therefore, extreme temperature events in the Reanalysis data tend to cover larger spatial extents and form more coherent spatial clusters. The differences in θ_5 between the two datasets are statistically significant across most grid points, as the estimated coefficients for the Reanalysis data fall outside the confidence interval for the Simulated data for all but 5 southerly points in \mathcal{F} . Both datasets show higher θ_5 values in regions with favorable conditions for heatwave persistence, such as low-lying plains.

5.1.2 Upper extremal range median θ_2

Since $\theta_2(\mathbf{s}; \mathcal{E}_{u_p}^{\mathcal{F}, X}, 0.5)$ represents the median of $R^*(\mathbf{s})$ conditioned on $\mathbf{s} \in \mathcal{E}_{u_p}^{\mathcal{F}, X}$, we leverage Generalized Additive Models (GAMs) to perform quantile regression (at the 50% level) on $\log R^*(\mathbf{s})$ whenever the logarithm is well-defined. Specifically, we use smooth splines to model spatial coordinates as covariates, capturing non-linear spatial trends, while imposing a linear dependence on $\log(-\log(1-p))$ to reflect the relationship with the threshold level p . This modeling strategy would allow adding other covariates related to topography (*e.g.*, elevation), or the time of observation to account for time trends.

Figure 8 showcases the median upper extremal range $\theta_2(\mathbf{s}; \mathcal{E}_{u_p}^{\mathcal{F}, X}, 0.5)$ at the 99th percentile threshold of X . While both datasets demonstrate similar spatial patterns, the Simulation dataset generally displays smaller θ_2 values, reinforcing the observation of more localized extremes compared to the Reanalysis data.

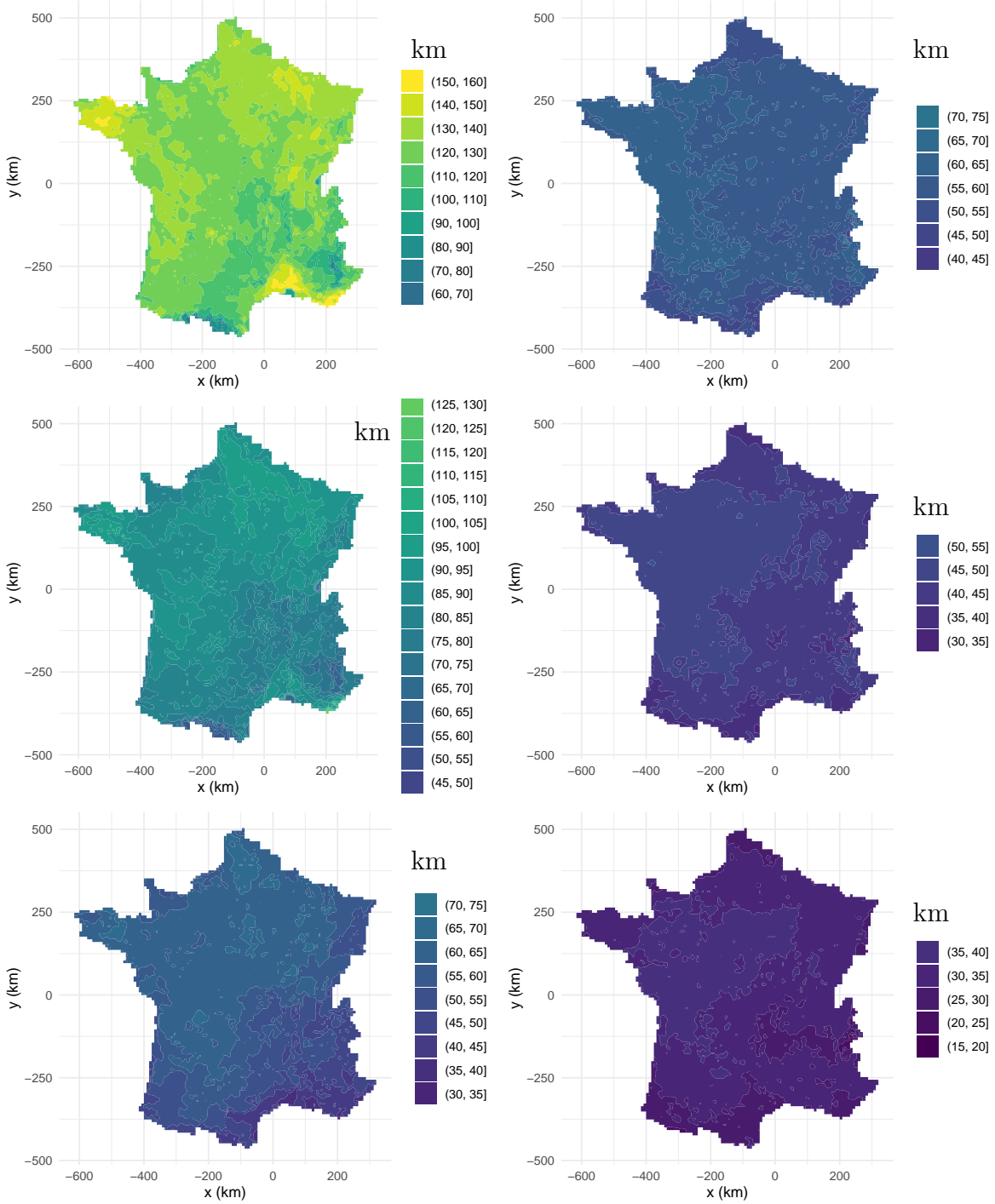


Figure 7: Estimated $\theta_5(\mathbf{s}; \mathcal{E}_{u_p}^{\mathcal{F}, X})$ (measured in km) for the Reanalysis (left column) and Simulation (right column) datasets at $p = 0.99$. The estimates are truncated at 160 km to enhance visualization. Top row: Upper end of the 95% confidence interval. Middle row: The estimate $\hat{\theta}_5(\mathbf{s}; \mathcal{E}_{u_p}^{\mathcal{F}, X})$. Bottom row: Lower end of the 95% confidence interval.

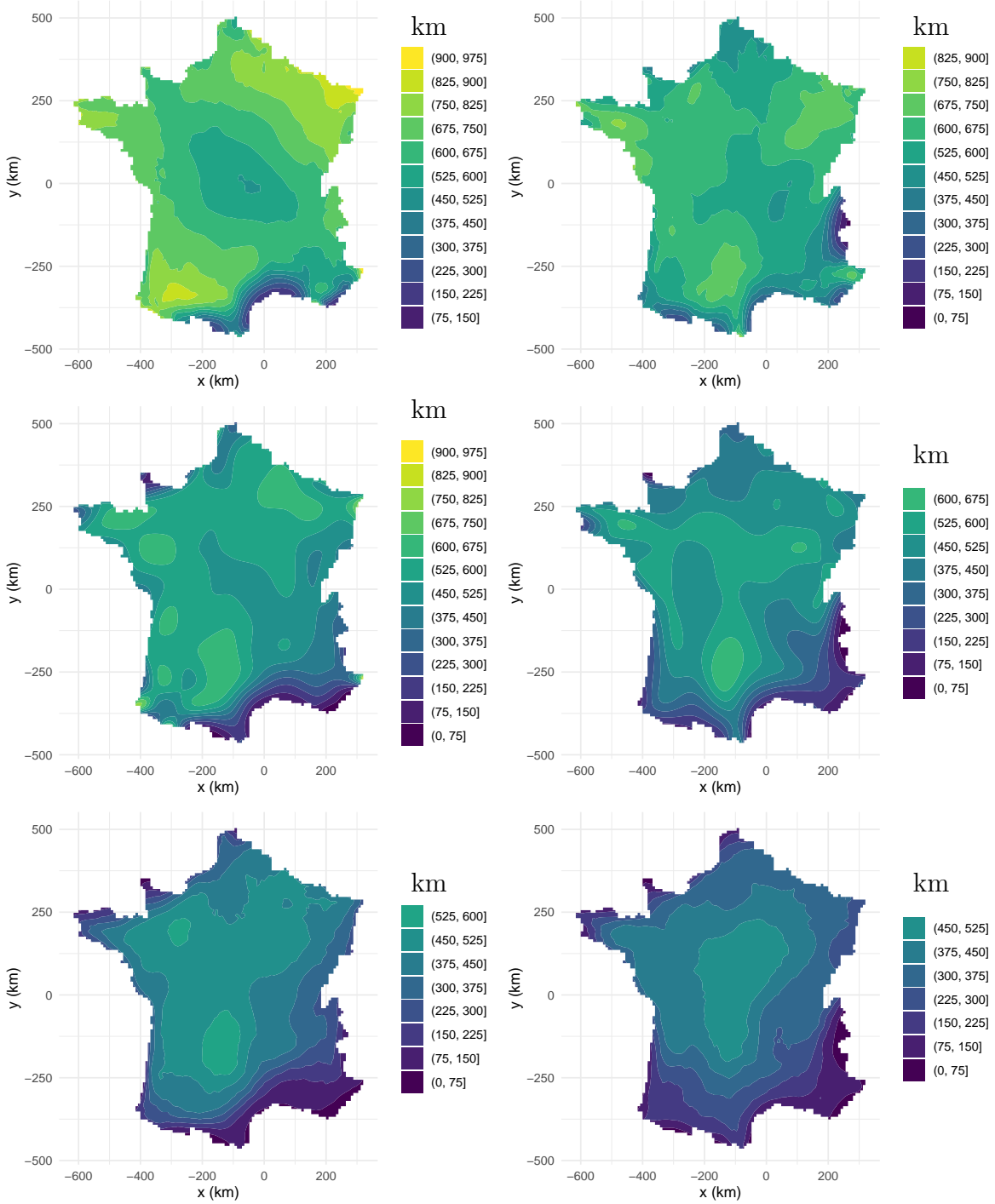


Figure 8: Estimated $\theta_2(\mathbf{s}; \mathcal{E}_{u_p}^{\mathcal{F}, X}, 0.5)$ (measured in km) for the Reanalysis (left column) and Simulation (right column) datasets at $p = 0.99$. Top row: Upper end of the 95% confidence interval. Middle row: The estimate $\hat{\theta}_2(\mathbf{s}; \mathcal{E}_{u_p}^{\mathcal{F}, X}, 0.5)$. Bottom row: Lower end of the 95% confidence interval. Left column: Reanalysis. Right column: Simulation.

The coefficient $\theta_2(\mathbf{s}; \mathcal{E}_{u_p}^{\mathcal{F}, X}, 0.5)$ provides a direct and interpretable measure of risk: it represents the median spatial extent of the connected component of the excursion set $\mathcal{E}_{u_p}^{\mathcal{F}, X}$ containing \mathbf{s} , conditional on $\mathbf{s} \in \mathcal{E}_{u_p}^{\mathcal{F}, X}$. In this case study, larger θ_2 values for the Reanalysis dataset suggest that extreme temperature events are more widespread, while the smaller values for the Simulation dataset indicate a more localized spatial footprint of extremes.

However, due to the relatively large size of the extremes in this case study, θ_2 is subject to edge effects, particularly near the boundaries of \mathcal{F} , where the connected component of the excursion set is truncated. The use of a GAM exacerbates these edge effects. Consequently, while θ_2 is well-suited for assessing spatial risk and has an intuitive interpretation, it is not optimal for evaluating the degree of asymptotic independence, where boundary and discretization biases can distort the scaling behavior at high thresholds.

For judging the degree of asymptotic independence, θ_5 is more appropriate, as it is less prone to edge effects and exhibits less variability in its estimators at a given threshold (see Table S1). Nonetheless, θ_2 remains a valuable complementary statistic, particularly for applications focused on risk quantification rather than asymptotic dependence analysis.

5.2 Estimating the scaling index β using θ_5

To better understand how the spatial extent of extremes scales as thresholds become more extreme, we focus on the area-perimeter ratio θ_5 for estimating the scaling index β . We follow the inference procedure outlined in Section 4.3. The scaling index provides a quantitative measure of asymptotic independence, with lower β indicating weaker asymptotic independence (or stronger spatial dependence remaining at high thresholds).

Figure 9 maps the estimated $\beta(\mathbf{s})$ for $\mathbf{s} \in \mathcal{F}$. The Reanalysis data has β values of generally lower magnitude, especially in regions such as low-lying plains known to be prone to

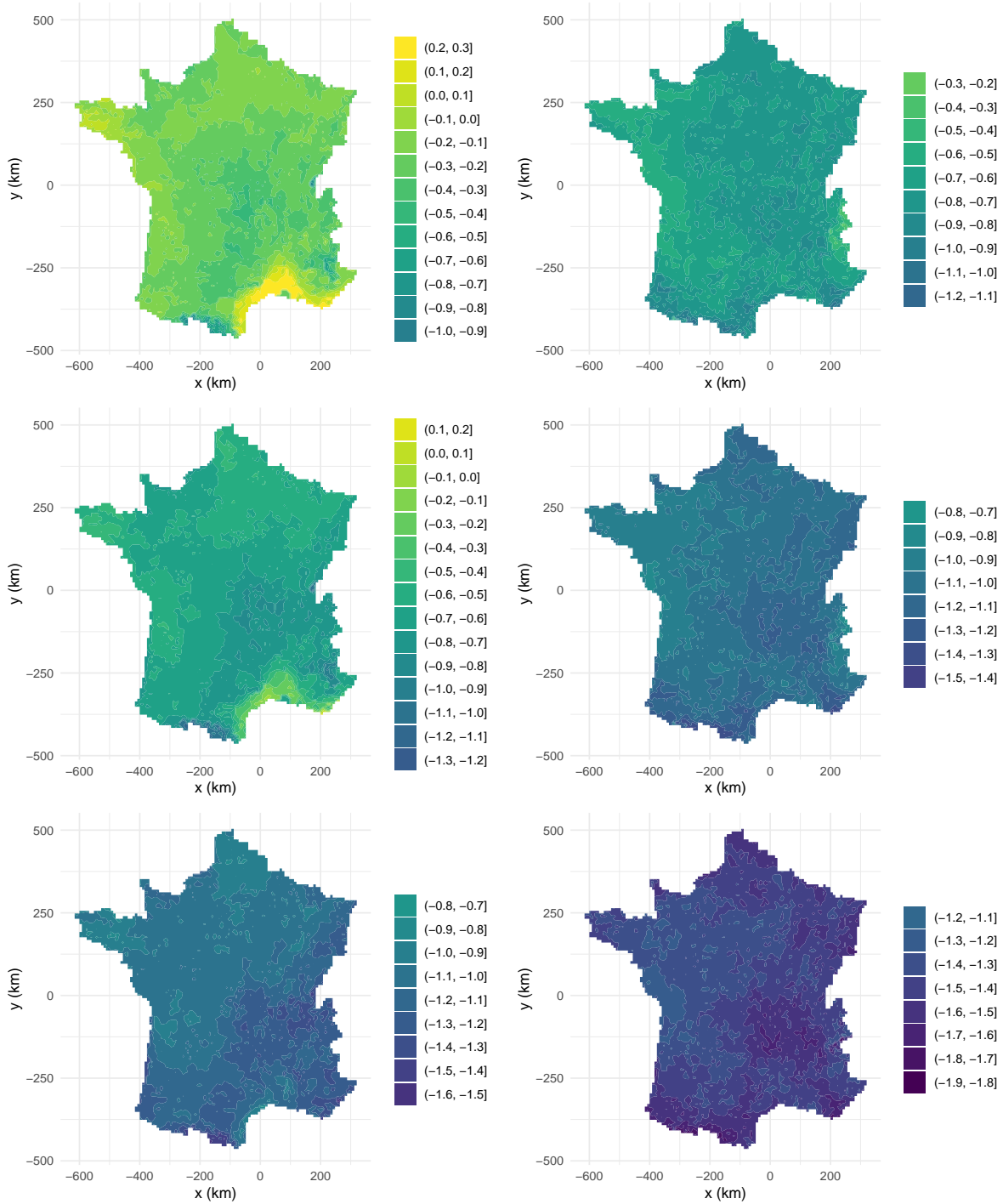


Figure 9: Spatial distribution of $-\beta(\mathbf{s})$, the negative scaling index inferred from $\theta_5(\mathbf{s}; \mathcal{E}_{u_p}^{\mathcal{F}, X})$, across mainland France. Top row: Upper end of the 95% confidence interval, indicating locations where asymptotic dependence cannot be rejected if the value is positive. Middle row: Estimated values of $-\beta(\mathbf{s})$. Bottom row: Lower end of the 95% confidence interval. Left column: Reanalysis dataset. Right column: Simulation dataset.

widespread heatwaves. In contrast, the Simulation data show higher β values uniformly, reflecting a tendency for extremes to become more localized as their intensity increases.

We can test the null hypothesis of asymptotic dependence. It cannot be rejected at a given location \mathbf{s} if the confidence interval for $-\beta(\mathbf{s})$ contains non-negative values, *i.e.*, if its upper bound, as shown in the top row of Figure 9, is positive. In Reanalysis data, asymptotic dependence cannot be rejected for areas near the Mediterranean coast in the South, where the confidence interval includes zero, suggesting weaker evidence of asymptotic independence in this region. However, for most other locations in mainland France, the confidence intervals exclude zero, allowing us to reject asymptotic dependence. In contrast, in Simulation data, asymptotic dependence is rejected everywhere.

6 Discussion

This work introduced local excursion-set coefficients to quantify the spatial extent and dependence of threshold exceedances in random fields. These coefficients provide interpretable measures of spatial dependence and enable new insights into the behavior of extremes, as demonstrated through theoretical analysis, simulations, and application to French temperature data. We have put focus on exceedances above relatively high marginal quantile levels and inference techniques for extrapolation towards very extreme levels, which is typically a challenging task. However, the coefficients we propose could also provide relevant information at intermediate levels, for example when the threshold corresponds to marginal medians where excursion sets would cover on average half of the study domain. If data are not organized on a fine regular grid in metric units, they could be preprocessed using interpolation methods (*e.g.*, kriging, basis-functions techniques).

The choice of an appropriate θ_k depends on several factors. The scale of extremes relative

to the spatial domain is crucial, ensuring minimal discretization and truncation error. Applications that prioritize risk aversion may favor more conservative coefficients like θ_2 . Additionally, the resolution of the grid affects estimates, with coarser grids potentially introducing biases that influence the choice of θ_k . Finally, in scenarios where connectivity is critical, θ_5 has the drawback that it does not directly assess connected regions. While this work focused on five illustrative examples, the general framework in Definition 4 allows for a vast number of coefficients tailored to specific needs.

Strong links arise between the intrinsic volumes of unconditional excursion sets and the spatial extent of conditional extremes (Cotsakis, Di Bernardino & Opitz 2024). This connection highlights the theoretical foundation of our coefficients and their potential for broader application in stochastic geometry. Our work illustrates links between spatial extreme-value theory, stochastic geometry, and topological data analysis, and presents opportunities for further research to develop statistical tools for analyzing large-scale climate data.

The application to French temperatures revealed significant differences between Reanalysis and Simulation data. By estimating the scaling index β using θ_5 , we showed that extremes in the Simulation dataset were more localized, indicating stronger asymptotic independence compared to the Reanalysis dataset. Additionally, we estimated θ_2 , a very conservative measure of spatial risk, emphasizing its utility for practical risk assessment. Generalized Additive Models, as used with spatial position as covariate for θ_1 or θ_2 could further incorporate other covariates like elevation, time, or large-scale atmospheric conditions (similar to Zhong et al. 2024, Koh et al. 2024) to infer more general nonstationary behavior. Moreover, applications to variables other than temperature could be explored. In future work, these coefficients could guide the construction of random field models exhibiting spatial nonstationarity in the dependence structure of extremes, such as deter-

mining the choice of noise distribution and of kernel bandwidths in process convolutions (*i.e.*, in fields constructed by smoothing pixel-based white noise), for example by using estimated maps of θ_k as covariates. They also have applications in generative models, including neural networks on grids, where they can capture spatial dependence in nonstationary generative processes like stable diffusion. Other useful methodological extensions would be to extend the definition of coefficients to spatiotemporal settings and multivariate processes, and develop connections to topological data analysis, ultimately enhancing the toolbox for studying climate extremes and informing decision-making.

References

- Adler, R. J. & Taylor, J. E. (2007), *Random fields and geometry*, Springer Monographs in Mathematics, Springer, New York.
- Bolin, D. & Lindgren, F. (2015), ‘Excursion and contour uncertainty regions for latent Gaussian models’, *Journal of the Royal Statistical Society: Series B (Statistical Methodology)* **77**(1), 85–106.
- Bolin, D. & Lindgren, F. (2018), ‘Calculating probabilistic excursion sets and related quantities using excursions’, *Journal of Statistical Software* **86**(5), 1–20.
- Coles, S., Heffernan, J. & Tawn, J. (1999), ‘Dependence measures for extreme value analyses’, *Extremes* **2**, 339–365.
- Cotsakis, R., Di Bernardino, E. & Duval, C. (2024), ‘Surface area and volume of excursion sets observed on point cloud based polytopic tessellations’, *The Annals of Applied Probability* **34**(3), 3093 – 3124.

- Cotsakis, R., Di Bernardino, E. & Opitz, T. (2024), ‘On the spatial extent of extreme threshold exceedances’, *Preprint arXiv:2411.02399* .
- Davis, R. A. & Mikosch, T. (2009), ‘The extremogram: A correlogram for extreme events’, *Bernoulli* **15**(4), 977–1009.
- Hult, H. & Lindskog, F. (2005), ‘Extremal behavior of regularly varying stochastic processes’, *Stochastic Processes and their Applications* **115**(2), 249–274.
- Hult, H. & Lindskog, F. (2006), ‘Regular variation for measures on metric spaces’, *Publications de l’Institut Mathématique* **80**(94), 121–140.
- Huser, R., Opitz, T. & Wadsworth, J. (2024), ‘Modeling of spatial extremes in environmental data science: Time to move away from max-stable processes’, *Preprint arXiv:2401.17430* .
- Huser, R. & Wadsworth, J. L. (2022), ‘Advances in statistical modeling of spatial extremes’, *Wiley Interdisciplinary Reviews: Computational Statistics* **14**(1), e1537.
- Kabluchko, Z., Schlather, M. & de Haan, L. (2009), ‘Stationary max-stable fields associated to negative definite functions’, *The Annals of Probability* **37**(5), 2042 – 2065.
- Koh, J., Koch, E. & Davison, A. C. (2024), ‘Space-time extremes of severe U.S. thunderstorm environments’, *Journal of the American Statistical Association* pp. 1–24.
- Perkins, S., Alexander, L. & Nairn, J. (2012), ‘Increasing frequency, intensity and duration of observed global heatwaves and warm spells’, *Geophysical Research Letters* **39**(20).
- Politis, D. N. & Romano, J. P. (1994), ‘The stationary bootstrap’, *Journal of the American Statistical Association* **89**(428), 1303–1313.

- Schlather, M. & Tawn, J. A. (2003), ‘A dependence measure for multivariate and spatial extreme values: Properties and inference’, *Biometrika* **90**(1), 139–156.
- Sethian, J. A. (1996), ‘A fast marching level set method for monotonically advancing fronts’, *Proceedings of the National Academy of Sciences* **93**(4), 1591–1595.
- Strokorb, K., Ballani, F. & Schlather, M. (2015), ‘Tail correlation functions of max-stable processes: Construction principles, recovery and diversity of some mixing max-stable processes with identical TCF’, *Extremes* **18**, 241–271.
- Tawn, J., Shooter, R., Towe, R. & Lamb, R. (2018), ‘Modelling spatial extreme events with environmental applications’, *Spatial Statistics* **28**, 39–58.
- Vidal, J.-P., Martin, E., Franchistéguy, L., Baillon, M. & Soubeyroux, J.-M. (2010), ‘A 50-year high-resolution atmospheric reanalysis over France with the Safran system’, *International journal of climatology* **30**(11), 1627–1644.
- Wadsworth, J. L. & Tawn, J. A. (2022), ‘Higher-dimensional spatial extremes via single-site conditioning’, *Spatial Statistics* **51**, 100677.
- Zhong, P., Brunner, M., Opitz, T. & Huser, R. (2024), ‘Spatial modeling and future projection of extreme precipitation extents’, *Journal of the American Statistical Association* pp. 1–16.

Supplementary materials

To aid in the interpretation of our coefficients, Figure S10 illustrates the random variables $R_*(\mathbf{s})$ and $R^*(\mathbf{s})$, which are used in the construction of the coefficients θ_1 and θ_2 , respectively. Specifically, $R_*(\mathbf{s})$ represents the distance from \mathbf{s} to the nearest non-exceedance point in \mathcal{G} , while $R^*(\mathbf{s})$ represents the distance from \mathbf{s} to the furthest connected exceedance point within the same connected component of the excursion set $\mathcal{E}_u^{\mathcal{G},X}$ as \mathbf{s} .

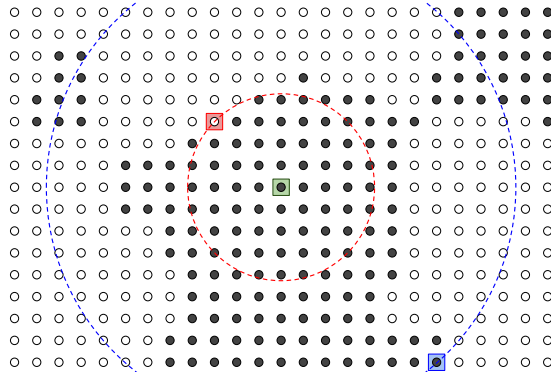


Figure S10: Illustration of excursion set geometry: the black points represent the excursion set $\mathcal{E}_u^{\mathcal{G},X}$ on a grid \mathcal{G} . The green point is the chosen reference location \mathbf{s} . The red circle indicates $R_*(\mathbf{s})$ and the blue one represents $R^*(\mathbf{s})$.

Table S1 below summarizes the median and standard deviation of the logarithm of the estimated coefficients θ_k across different ranges l and locations \mathbf{s} .

| θ | l (range) | \mathbf{s} | Median of θ | S.d. of $\log \theta$ |
|------------|-------------|--------------|--------------------|-----------------------|
| θ_1 | 30 | $\mathbf{0}$ | 4.7 | 0.073 |
| | 30 | $(60, 0)'$ | 6.0 | 0.051 |
| | 120 | $\mathbf{0}$ | 17.0 | 0.057 |
| | 120 | $(60, 0)'$ | 19.3 | 0.063 |
| θ_2 | 30 | $\mathbf{0}$ | 33.3 | 0.029 |
| | 30 | $(60, 0)'$ | 30.7 | 0.035 |
| | 120 | $\mathbf{0}$ | 84.9 | 0.000 |
| | 120 | $(60, 0)'$ | 85.6 | 0.034 |
| θ_3 | 30 | $\mathbf{0}$ | 18.9 | 0.025 |
| | 30 | $(60, 0)'$ | 21.2 | 0.032 |
| | 120 | $\mathbf{0}$ | ∞ | NaN |
| | 120 | $(60, 0)'$ | 84.2 | 0.050 |
| θ_4 | 30 | $\mathbf{0}$ | 4.6 | 0.055 |
| | 30 | $(60, 0)'$ | 4.4 | 0.050 |
| | 120 | $\mathbf{0}$ | 16.7 | 0.060 |
| | 120 | $(60, 0)'$ | 14.0 | 0.061 |
| θ_5 | 30 | $\mathbf{0}$ | 18.8 | 0.021 |
| | 30 | $(60, 0)'$ | 19.3 | 0.021 |
| | 120 | $\mathbf{0}$ | 89.1 | 0.029 |
| | 120 | $(60, 0)'$ | 88.0 | 0.034 |

Table S1: Summary statistics of log-transformed coefficients for different spatial ranges l and locations \mathbf{s} . $\mathbf{s} = \mathbf{0}$ denotes the center of the grid, while $\mathbf{s} = (60, 0)'$ represents a boundary location. The range l indicates the spatial dependence scale in the simulation in Section 3.1.